Modeling Dynamic Functional Information Flows on Large-Scale Brain Networks

Peili Lv[1], Lei Guo[1], Xintao Hu[1], Xiang Li[2], Changfeng Jin[3], Junwei Han[1], Lingjiang Li[3], and Tianming Liu[2]

[1] School of Automation, Northwestern Polytechnical University, Xi'an, China
[2] Department of Computer Science and Bioimaging Research Center, The University of Georgia, Athens, GA, USA
[3] The Mental Health Institute, The Second Xiangya Hospital, Central South University, Changsha, China

Abstract. Growing evidence from the functional neuroimaging field suggests that human brain functions are realized via dynamic functional interactions on large-scale structural networks. Even in resting state, functional brain networks exhibit remarkable temporal dynamics. However, it has been rarely explored to computationally model such dynamic functional information flows on large-scale brain networks. In this paper, we present a novel computational framework to explore this problem using multimodal resting state fMRI (R-fMRI) and diffusion tensor imaging (DTI) data. Basically, recent literature reports including our own studies have demonstrated that the resting state brain networks dynamically undergo a set of distinct brain states. Within each quasi-stable state, functional information flows from one set of structural brain nodes to other sets of nodes, which is analogous to the message package routing on the Internet from the source node to the destination. Therefore, based on the large-scale structural brain networks constructed from DTI data, we employ a dynamic programming strategy to infer functional information transition routines on structural networks, based on which hub routers that most frequently participate in these routines are identified. It is interesting that a majority of those hub routers are located within the default mode network (DMN), revealing a possible mechanism of the critical functional hub roles played by the DMN in resting state. Also, application of this framework on a post trauma stress disorder (PTSD) dataset demonstrated interesting difference in hub router distributions between PTSD patients and healthy controls.

Keywords: structural brain networks, brain state changes, dynamic functional information flow, default mode network, post trauma stress disorder.

1 Introduction

The human brain is often described as a collection of specialized functional networks that flexibly interact with each other to support various perceptive, cognitive, or resting state functions [1]. From a computational perspective, such functional process essentially involves the participation of different brain areas in a temporal sequence, and also presents a spatial routine in structural brain networks. In this sense, the brain

K. Mori et al. (Eds.): MICCAI 2013, Part II, LNCS 8150, pp. 698–705, 2013.

network is analogous to the Internet, as both of them coordinate integral components to complete information processing and transition tasks. Essentially, the core components in a computational network, i.e., the routers and dynamic links on the Internet, are critical to understand its working principles and mechanisms. In this context, therefore, a key question in understanding the working mechanisms of functional brain networks is to find out the dynamic information transition routines and key router-like brain areas. Hence, in this paper, we are motivated to explore dynamic functional information transition routines and the hub routers that play key roles in functional brain network dynamics.

Recently, perceptive, cognitive, or resting state activities on brain networks are reported to be spanned by a set of distinct functional states [2-4]. A functional brain state is often defined as the quasi-stable interaction or synchronization between multiple cortical areas and the modulation of intrinsic circuits by feedback connection [5]. Growing evidence from the functional neuroimaging field [e.g., 2-3, 6-8] suggested that human brain functions are realized via dynamic functional interactions on large-scale structural networks. Even in resting state, functional brain networks exhibit remarkable temporal dynamics [2-4, 6]. Thus, it is reasonable to hypothesize that the temporal transition of the functional information in each distinct brain state exhibits a proprietary routine that is spatially distributed on the structural routers of the brain networks. Notably, there could possibly exist distinct causalities which drive the dynamic information transition among the brain networks in each functional state. Inspired by literature reports [e.g., 2-3, 6-8] and our observations, in this paper, we present a novel computational framework to explore the routines and routers of dynamic functional information transition on large-scale brain networks using multimodal DTI/R-fMRI data. In particular, we use a publicly available cortical landmarks localization system named Dense Individualized and Common Connectivity-based Cortical Landmarks (DICCCOL) [9] as a brain reference system for the representation of common human brain networks. The proposed computational pipeline that is composed of three steps will be detailed in Fig. 1. As an application example, we used the computational pipeline to investigate the difference of dynamic transition routines and routers between patients with post trauma stress disorder (PTSD) and matched normal controls, and interesting results were obtained.

2 Methods

2.1 DFCS and Temporal Brain State Extraction

In our study, we adopted the publicly available DICCCOL (http://dicccol.cs.uga.edu) brain reference and localization system [9] to localize large-scale structural brain networks. For each DICCCOL ROI, we extracted the corresponding R-fMRI signal Y_i for the i-th DICCCOL, Fig. 1(a). To construct the Dynamic functional Connectivity Strength (DFCS), a sliding window with width d=14 [3] was used to parcellate Y_i into temporal segments and the segment at time point t is:

$$S_{i,t} = \{Y_{i,tm} \mid t \le tm < t + d\} \tag{1}$$

Where $1 \le t \le 186$. For each pair of nodes i and j, the functional connectivity $FS_{i,j,t}$ between them at time point t is calculated as the Pearson correlation coefficient:

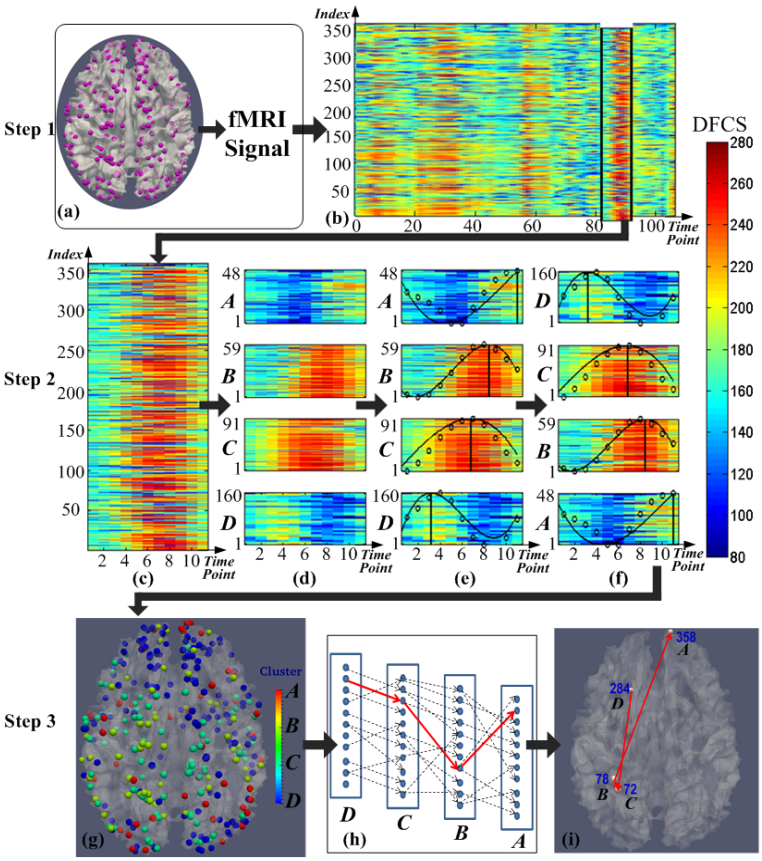

Fig. 1. The flowchart of the proposed framework. Step 1, 2 & 3 are described in subsection 2.1, 2.2 & 2.3, respectively. (a) Extraction of fMRI signal based on DICCCOL. (b) An exemplar DFCS profile of large-scale brain networks. (c) A brain state extracted from DFCS. (d) Brain state decomposition into N non-overlapped sub-networks (A-D for N=4 for example). (e) The activity peak (black bar) detection for each sub-network using a polynomial curve-fitting method. (f) Dynamic activation transitions among the sub-networks. (g) An exemplar visualization of the clustered sub-networks. (h) Illustration of routine tracing for a brain state. (i) An exemplar visualization of the traced routine.

$$FS_{i,j,t} = \begin{cases} corr(S_{i,t}, S_{j,t}) & i \neq j \\ 0 & otherwise \end{cases} \tag{2}$$

The dynamic functional connectivity strength (DFCS) for node i at time point t is calculated as:

$$DFCS_{i,t} = \sum_{j=1}^{358} FS_{i,j,t} \tag{3}$$

In general, $DFCS_{i,t}$ measures the overall functional interaction between node i and the rest of the ROIs at time t. It was used as a global measurement of the functional activity of the ROI in consideration, which has been adopted in the literature [3].

The extraction of the temporally changing brain states follows the similar semi-automatic methods described in [3-4]. Then, an effective sparse coding algorithm [10] was employed to learn the representative dictionary for the semi-automatically parcellated segments. As a result, each *DFCS* at time point *t* is assigned with a label by the sparsely represented dictionary (18 elements in total). The whole *DFCS* is then assigned with 18 different dictionary labels, and each corresponds to a center matrix representing the whole-brain network connectivity for corresponding labeled time points, which will be used in section 2.3. The continuous DFCS segment with the same labels for more than 10 time points (considered as sufficiently long segments) are extracted as a quasi-stable state, Fig. 1(b). At last, we obtained 101 states for the normal control group and 93 states for the PTSD patient group (details of the datasets in section 3). Mathematically, denote $DFCS_i=\{DFCS_{i,t}|t=1,2,\ldots,l\}$ as the DFCS vector of the *i*-th ROI within a state, *l* is temporal length of the state.

2.2 Dynamic Information Transition on Brain Networks

In each temporally separated quasi-stable brain state, the dynamic transition of functional activities of the ROIs may follow quite different routines. Since the timing order of functional activities is widely considered to reflect the causal effect in the neuroimaging field, e.g., in Granger Causality Modeling [11, 12], we then investigate the timing orders of synchronous activities among different sub-networks in each brain state. To model the dynamic transition of the activities of the ROIs in a given brain state, we cluster the 358 DICCCOL ROIs into non-overlapped sub-networks based on their DFCS similarities, Fig. 1(d). Here, our premise is that the subset of ROIs with temporally similar DFCS tends to be within the same sub-network, which has been commonly adopted as the criterion of functional network identification in the neuroimaging field [2, 6].

For the *m*-th state, the *k*-means clustering algorithm is adopted to group the 358 DICCCOL ROIs into *N* sub-networks (clusters). Denote G_n as the *n*-th sub-network. Denote $\overline{DFCS}^{(n)}$ as the mean of *DFCS* of G_n.

$$\overline{DFCS}^{(n)} = \frac{1}{|G_n|}\sum_{i\in G_n} DFCS_i \tag{4}$$

Here $|G_n|$ is the total number of ROIs in sub-network G_n.

The causal relationship among the extracted sub-networks is inferred by the temporal activity orders. That is, the activity of a sub-network might induce the activity of another sub-network, and results in the dynamic activity transitions among the sub-networks. In order to model the temporal activity transition patterns among the sub-networks, the temporal activity peak in each sub-network is detected. We fit $\overline{DFCS}^{(n)}$ using a cubic polynomial function $f(x)$, Fig. 1(e). Then, the temporal activation peak point $T^{(n)}$ of sub-network G_n is detected as:

$$T^{(n)} = \begin{cases} q & f'(q)=0, f''(q)<0, 0<q<l \\ \arg\max_t(\overline{DFCS}t^{(n)}) & otherwise \end{cases} \tag{5}$$

where $T^{(n)}$ takes the cubic function maxima *q* if *q* is located in the segment time interval [0, *l*]. Otherwise, it takes the maximum value point of $\overline{DFCS}^{(n)}$. After temporal activity peak detection, the activities of the *N* sub-networks in the *m*-th brain state are

temporally sorted, Fig. 1(f), in which the concept is similar to the temporal causality modeling [11, 12], in order to infer the dynamic functional information flows among the sub-networks.

2.3 Temporal Information Transition Routine Modeling

To represent the routine consisting of network ROIs, we select one node from each sub-network as the "router", so the routine consists of N nodes from N sub-networks in a brain state that could represent the activation transitions of the corresponding state, Fig. 1(h)-(i). As described in section 2.1, by using a sparse coding method [10], we encoded the functional connectivity pattern through the whole time series at each point into 18 discrete and common functional connectivity (CFC) matrices. As a result, each functional brain state now corresponds to a CFC matrix.

The causal relationship among sub-networks might rely on the functional interaction among a specific set of ROIs. We hypothesize that the optimal routine should not contain weak connectivity that harms the overall efficiency, which could be obtained by maximizing the multiplication of functional connectivity between each two consecutive ROIs located in the transition path, as it has much less tolerance to a single weak connectivity. Denote $E=\{e_{ij}|i,j=1,2,\ldots,358\}$ as the edge set in brain network, $CFC(e_{ij})$ as the element of the CFC matrix of the corresponding state, which represents the functional interaction between ROI i and j in the specific state.

In the n-th activated sub-network G_n. P is the multiplication of the edges between N sub-networks. $L=\{e_{ij}|i\in G_n, j\in G_{n+1}, 1\le n<N\}$ is the routine. Since the high interaction between the ROIs from different sub-networks predicts the transition of the activity, the routine that the transition of the activities follows is detected as:

$$P=\prod_{n=1}^{N-1} CFC(e_{ij}),\ \ i\in G_n, j\in G_{n+1} \tag{6}$$

$$L=\arg\max_{L}\{P\} \tag{7}$$

Eq. (7) is solved by the dynamic programming method [13]. The two steps of the algorithm are briefly summarized as follows.

Step 1 (Recursion):

$$P_{1,i}=1 \tag{8}$$

$$P_{n,j}=\max_{i\in G_{n-1}}(P_{n-1,i}\times e_{ij}) \tag{9}$$

$$Ptr(n,j)=\arg\max_{i\in G_{n-1}}(P_{n-1,i}\times e_{ij}) \tag{10}$$

Step 2 (Routine back tracking):

$$x_N=\arg\max_{i\in G_N}(P_{N,i}) \tag{11}$$

$$x_{n-1}=Ptr(n,x_n) \tag{12}$$

$P_{n,j}$ is the maximization of multiplication of functional connectivity from the first sub-network until the j-th ROI in the n-th sub-network ($j\in G_n$), with one node from each previous activated sub-network. Here, x_n represents the n-th nodes (selected from the n-th sub-network) located in the routine. In this algorithm, the routine is retrieved by saving back pointers that remember which ROI was used in Eq. (9). $Ptr(n,j)$ is the back pointer function that returns the ROI i that maximizes Eqs. (9) and (10).

2.4 Routers Identification

The probability that a given ROI is a router is inferred as the frequency that the network ROI occurs in the detected routines. Denote M as the total number of states of the dataset (M=101 for the normal control dataset and M=93 for the PTSD patient). And for the m-th state, denote $\delta_i^{(m)}$ as the label that indicates the i-th ROI's occurrence in the m-th state. Denote δ_i as the overall router frequency of i-th ROI in all the M states normalized by dividing $M \times N$.

$$\delta_i^{(m)} = \begin{cases} 1 & i \in V^{(m)} \\ 0 & otherwise \end{cases}, \quad \delta_i = \frac{1}{M \times N} \sum_{m=1}^{M} \delta_i^{(m)} \tag{13}$$

$V^{(m)}$ is the set of nodes in the routine for the m-th state. N is the parameter of number of sub-networks.

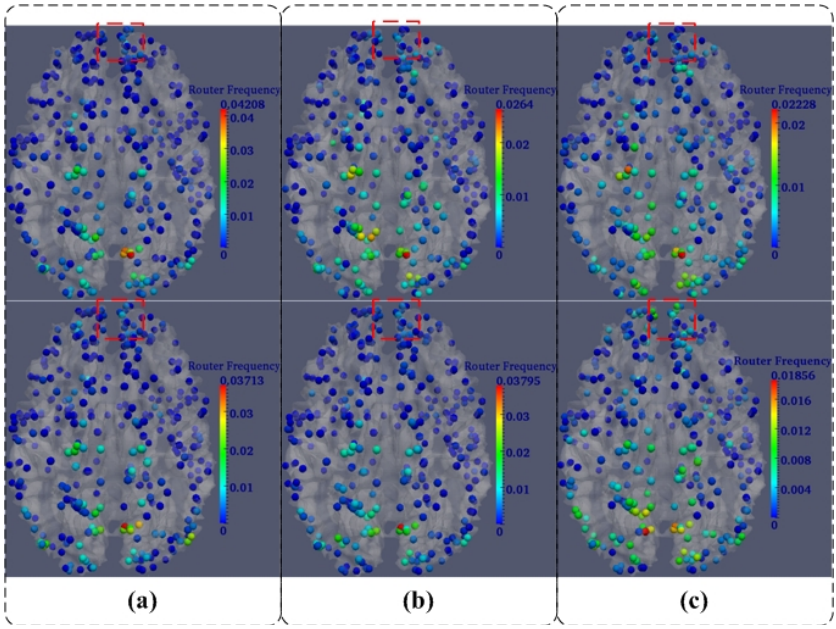

Fig. 2. Router frequency comparison between normal controls and PTSD patients. The upper panel is for control subjects and the bottom panel is for patient subjects. (a), (b) and (c) corresponds to results with the number of clusters as 4, 6, and 8.

3 Results

The methods in section 2 have been applied on the following dataset. Post-traumatic stress disorder (PTSD) patients and controls were recruited under IRB approvals. Multimodal DTI and R-fMRI datasets for 98 subjects including 53 adult normal controls and 45 adults PTSD patients were acquired on a 3T MRI scanner. Acquisition parameters for the scans were as follows. R-fMRI: 64×64 matrix, 4mm slice thickness, 220 mm FOV, 30 slices, TR=2s; DTI: 256×256 matrix, 3mm slice thickness, 240mm FOV,

50 slices, 15 DWI volumes, b-value = 1000. Pre-processing steps of the DTI and R-fMRI datasets are referred to methods in [3-4].

3.1 Frequent Router Comparison of PTSD Patient and Normal Control

The frequencies that the DICCCOL ROIs occurred in the detected routines are quantitatively measured. Fig. 2 shows the normalized router frequency δ_i described in subsection 2.4 on PTSD patient and healthy control datasets. The result shows the overall consistency and reproducibility, as well as noticeable difference between normal control and PTSD patients. In Fig. 2, it is clear that the distribution of frequent routers among PTSD patient subjects is more widespread. In particular, some area, e.g., the anterior area (shown in dashed red box), are detected with higher router frequency among PTSD patient subjects than normal control subjects, which is in agreement with previous literature reports that anterior areas are involved in the neural circuitries in PTSD and they are hyper-active [14, 15].

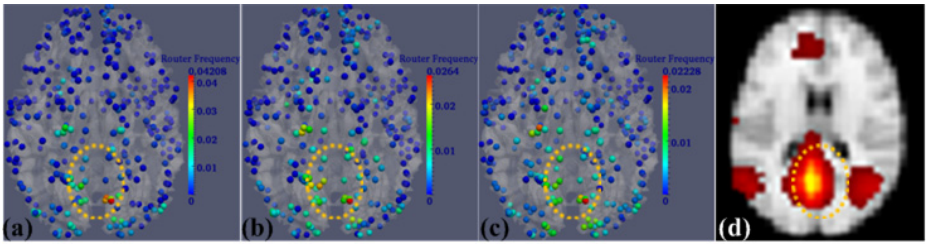

Fig. 3. Neuroscience interpretation of frequent routers. (a)-(c) Frequent routers located in the DMN, with number of clusters as 4, 6 and 8 respectively. The color-bars are on the right side. (d) Volumetric image with the default mode network.

3.2 Neuroscience Interpretation of Frequent Routers

We performed the same analysis (section 2) on all of 101 brain states (section 3.1) in the normal controls and summarized the results in Figs. 3(a)-(c). It is interesting that a majority of most frequent router nodes are located within the default mode network (DMN) [16], particularly the posterior cingulate cortices, as highlighted by the orange oval shapes. For visual comparison purpose, a volumetric image showing the DMN peak nodes derived from applying group-wise ICA [17] on R-fMRI data is provided in Fig. 3(d). Our result in Figs. 3(a)-(c) is quite consistent with current literature reports on the vital roles played by the DMN in resting state functional activities [16, 18]. Importantly, our work from a dynamic functional information flow perspective reveals a possible novel mechanism of DMN: it serves as the functional information transition hub, as demonstrated in Figs. 3(a)-(c).

4 Conclusion

In this paper, we presented a novel computational framework to explore the routines and frequent routers of dynamic functional activity transitions in large-scale brain

networks. Experimental results have shown that our methods and results are reproducible and robust to different datasets and experimental parameters. Importantly, our results demonstrated a possible mechanism of the DMN in regulating functional activities in resting state: it possibly serves as the hub for functional information transition. The framework was also applied on multimodal DTI/R-fMRI datasets of PTSD patients and matched normal controls, and meaningful difference of the router frequency between PTSD patients and the normal controls was observed.

References

1. Fair, D.A., Cohen, A.L., Power, J.D., et al.: Functional Brain Networks Develop from a "Local to Distributed" Organization. PLoS Computational Biology 5(5) (2009)
2. Smith, S.M., Miller, K.L., Moeller, S., et al.: Temporally-independent functional modes of spontaneous brain activity. PNAS 109(8), 3131–3136 (2012)
3. Li, X., et al.: Detecting Brain State Changes via Fiber-Centered Functional Connectivity Analysis. Neuroinformatics (2012)
4. Zhang, X., et al.: Characterization of Task-free/Task-performance Brain States. In: Ayache, N., Delingette, H., Golland, P., Mori, K. (eds.) MICCAI 2012, Part II. LNCS, vol. 7511, pp. 237–245. Springer, Heidelberg (2012)
5. Gilbert, C.D., Sigman, M.: Brain States, Top-Down Influences in Sensory Processing. Neuron 54, 677–696 (2007)
6. Chang, C., Glover, G.H.: Time-frequency dynamics of resting-state brain connectivity measured with fMRI. NeuroImage 50(1), 81–98 (2010)
7. Majeed, W., et al.: Spatiotemporal dynamics of low frequency BOLD fluctuations in rats and humans. NeuroImage 54, 1140–1150 (2011)
8. Bassett, D.S., et al.: Dynamic reconfiguration of human brain networks during learning. PNAS 108(18), 7641–7646 (2011)
9. Zhu, D., Li, K., Guo, L., et al.: DICCCOL: dense individualized and common connectivity-based cortical landmarks. Cerebral Cortex 23(4), 786–800 (2013)
10. Yang, M., Zhang, L., Feng, X., Zhang, D.: Fisher Discrimination Dictionary Learning for Sparse Representation. In: ICCV, Barcelona, pp. 543–550 (2011)
11. Friston, K.J.: Functional and effective connectivity in neuroimaging: a synthesis. Hum. Brain Mapp. 2, 56–78 (1994)
12. Seth, A.K.: A MATLAB toolbox for Granger causal connectivity analysis. J. Neurosci. Meth. 186(2), 262–273 (2010)
13. Forney, G.D.: The Viterbi algorithm. Proceedings of the IEEE 61(3), 268–278 (1973)
14. Francati, V., et al.: Functional neuroimaging studies in posttraumatic stress disorder: review of current methods and findings. Depression and Anxiety 24(3), 202–218 (2007)
15. Shin, L.M., et al.: Resting metabolic activity in the cingulate cortex and vulnerability to posttraumatic stress disorder. Arch Gen Psychiatry 66(10), 1099–1107 (2009)
16. Fox, M.D., Raichle, M.E.: Spontaneous fluctuations in brain activity observed with functional magnetic resonance imaging. Nat. Rev. Neurosci. 8, 700–711 (2007)
17. `http://mialab.mrn.org/software/gift/index.html`
18. Raichle, M.E., Snyder, A.Z.: A default mode of brain function: A brief history of an evolving idea. NeuroImage 37(4), 1083–1090 (2007)